

Anodic and Cathodic Polarization of 1018 Mild Steel and 304 Stainless Steel

MSE 130: Experimental Materials Science and Design

Jonathan Lee

Department of Materials Science and Engineering
University of California, Berkeley

12 October 2020

Contents

1	Abstract	3
2	Introduction	3
2.1	Three Models for Polarization Curve Fitting	3
2.2	Additional Behavior: 1018MS	6
2.3	Additional Behavior: 304SS	6
2.4	Charactization Targets	7
3	Experimental Procedure	7
4	Results	9
5	Discussion	9
6	Conclusions	9
7	Acknowledgments	9
8	Appendix 1: Analysis Code	9
9	Appendix 2: Surface Microscopy	9

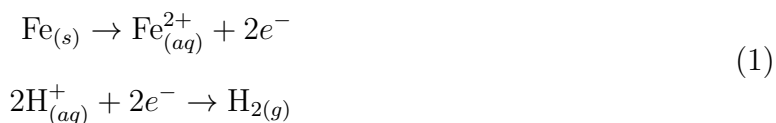
1 Abstract

2 Introduction

The purpose of this report is to quantify the corrosion behavior of rod samples of 1018 mild carbon steel ("1018MS") and 304 stainless steel ("304SS") when polarized in strongly acidic solutions. In particular, the manufacturer has requested characterization in 1M HCl and 1M H₂SO₄, both of which have a pH of ~0, but which manifest different passivation behaviors at higher potentials due to their anion species.

2.1 Three Models for Polarization Curve Fitting

When a metal is placed in solution, there often exists a difference between the metal's work function and the electron energy levels of the solution species. Electrons will therefore transfer between the metal and the solution. Depending on the properties of the resulting metal ions, this may result in the corrosion (dissolution) of the metal body. For example, for the coupled reactions in Equation 1, the Fe²⁺ ions produced are soluble in aqueous solution:



In an isolated system, this redox reaction continues until a the unfavorable charge imbalance cancels the driving force; an equilibrium electrochemical potential difference is thus established. Yet the scenario is modified if this metal electrode is connected to a counter-electrode of a different metallic species. The counter-electrode may manifest its own redox reactions so as to maintain charge neutrality in the solution; furthermore, any electrochemical potential difference between the electrode and counter-electrode provides a driving force for current flow. The net effect is that a circuit is established that continuously corrodes the

electrode.

This scenario is common in engineering situations – for example, the field of marine electronics deals heavily with the fact that the ocean-immersed components of a ship’s hull will corrode if made of dissimilar metals. In the laboratory, it may be replicated within a polarization cell, wherein a sample is immersed in solution with a counter-electrode (typically Pt, which does not corrode) and a reference electrode against which to measure potential differences (such as the Saturated Calomel Electrode, a Hg-based electrode abbreviated as ”SCE”). A potentiostat is used to drive the sample to various potentials relative to SCE; the current required to do so provides a measure of the reactions taking place at the sample surface. Such data sweeps are known as polarization curves.

The corrosion behavior of Fe in acidic solution may be described using the Butler-Volmer equation:

$$j = j_{\text{corr}} \left[\exp \left(\frac{\beta n F}{RT} (\phi - \Delta\phi_{\text{corr}}) \right) - \exp \left(\frac{(1 - \beta) n F}{RT} (\phi - \Delta\phi_{\text{corr}}) \right) \right] \quad (2)$$

In this form of the Bulter-Volmer equation, ϕ is the applied potential relative to SHE. $\Delta\phi_{\text{corr}}$ is the ”corrosion potential,” at which the rates of Fe oxidation and H reduction at the electrode are equal to each other. The reaction rate at this point is the corrosion rate j_{corr} and manifests as a point where zero current need be supplied by the potentiostat. β encodes any anisotropy between the exchange current densities of the anodic and cathodic reactions and is typically ~ 0.5 ; $n = 2$ is the number of electrons exchanged in the reaction; R is the ideal gas constant; F is the Faraday constant; and T is temperature.

In this analysis, the Bulter-Volmer equation will not be used in its full form, but instead in three separate modified forms. The first modification is to condense and rewrite the prefactors:

$$j = j_{\text{corr}} \left[\exp \left(\frac{\ln(10)\eta}{A_{\text{Fe}}} \right) - \exp \left(\frac{\ln(10)\eta}{A_{\text{H}}} \right) \right] \quad (3)$$

In this case, η is shorthand for the overpotential $\phi - \Delta\phi_{\text{corr}}$. A_{Fe} and A_{H} are the Tafel slopes

for Fe oxidation and H reduction, respectively, and may be considered as the overpotential required (in volts) to increase the reaction current density by a factor of 10. Fitting 3 to the polarization curve is typically done in the space of $\log_{10} |j|$ vs. η , such that either the anodic or cathodic terms dominate and produce linear behavior far from $\Delta\phi_{corr}$, while a singularity exists at $\Delta\phi_{corr}$ itself.

The second modification is to consider the Butler-Volmer equation in the small- η regime, i.e. at potentials close to $\Delta\phi_{corr}$ vs. SHE. A Taylor expansion of Equation 2 reveals linear behavior:

$$j = j_{corr} \frac{nF}{RT} \eta \quad (4)$$

For the Fe/H corrosion couple, the nF/RT prefactor has a value of 77.85 V^{-1} at 25°C . The corrosion potential may therefore be determined by a linear fit to a "Linear Polarization Resistance" (LPR) scan at small overpotentials (colloquially defined as $|\eta| < 100 \text{ mV}$).

The third modification is to account for the limitations of ion diffusion: at large overpotentials, a diffusion barrier may slow the rate of reaction, producing a smaller current than would be expected from Equation 2. Such diffusion barriers comprise complicated effects such as charge double-layers and may manifest themselves nonlinearly due to reaction kinetics, but as a rudimentary approximation, the barrier is assumed to have a constant resistivity ρ_{bar} . As such, a given half-reaction in Equation 2 will tend towards ohmic behavior at high currents, while Equation 2 itself describes electrical behavior comparable to a diode. The model in Reference [1] for a diode and resistor in series may be used as a guide to derive:

$$j = \frac{1}{B_0 \rho_{bar}} W(B_0 j_0 \rho_{bar} \exp(B_0 \eta)) \quad (5)$$

In this equation, B_0 is defined as $\ln(10)/A_0$ where A_0 is the Tafel-slope of the half-reaction, while W_0 is the 0-th branch of the Lambert W function. Since this equation is presented for a half-reaction, the parameters are defined in terms of a reference potential $\Delta\phi_{ref}$ and reference current j_0 instead of a corrosion potential and current, which only have meaning

for a reaction couple.

2.2 Additional Behavior: 1018MS

1018MS (0.15-0.20 wt% C, 0.60-0.90 wt% Mn, bal. Fe) possesses a heterogenous microstructure consisting of a nearly-carbonless ferrite α -phase and the high-carbon Fe_3C cementite phase. The fabrication of this steel involves quenching through a two-phase $\alpha + \gamma$ region; as a result, the original volumes of γ -phase become "pearlite," comprising dense lamellae of ferrite and cementite. An inspection of the Fe phase diagram for 0.18 wt% C indicates that 1018MS globally contains 2.7 wt% cementite, concentrated within pearlite regions that comprise 20 wt% of the microstructure. Cementite therefore comprises 14 wt% of the pearlite regions. For this analysis, the alloying element Mn is ignored.

This microstructure is generally expected to have a pronounced effect on the corrosion behavior of 1018MS. Cementite does not corrode as the high-Fe α -phase does, yet it conducts metallicity and catalyzes the H^+ reduction reaction. Specifically, the exchange current density on Fe_3C for hydrogen reduction is several orders of magnitude higher than on the α -phase. As the α -phase corrodes away, Fe_3C lamellae are left behind, producing a large increase in the area available for Fe_3C to catalyze the reaction. This means that as the 1018MS electrode corrodes, the parameters of Equation 3 should shift towards greater corrosion currents in the cathodic regime.

2.3 Additional Behavior: 304SS

304SS (18 wt% Cr, 8 wt% Ni, bal. Fe) is designed to self-passivate in acidic solution above certain overpotentials. Specifically, at a passivation potential $\Delta\phi_{\text{pass}} > \Delta\phi_{\text{corr}}$, Cr atoms oxidize into a +3 state in the form of a "passivation layer" consisting primarily of Cr_2O_3 . Despite being only a few unit cells thick, this passivation layer provides an extremely-effective barrier against continued Fe oxidation; above the $\Delta\phi_{\text{pass}}$, the electrode current in a passivation sweep is nearly flat.

This passivated regime, however, has an upper limit resulting from a "breakdown potential" ($\Delta\phi_{\text{breakdown}}$) at which Cr_2O_3 begins to oxidize into aqueous HCrO_4^- ions (+6 Cr oxidation state). In the presence of chloride ions, the limit is instead dictated by "pitting potential" ($\Delta\phi_{\text{pit}}$), wherein Cl^- ions locally attack the passivation barrier in a self-catalyzed reaction, thus locally restoring Fe corrosion behavior. This pitting potential typically occurs before the passivation layer breakdown potential; as such, the passivation regime in HCl is expected to be smaller than in H_2SO_4 .

2.4 Characterization Targets

In light of the above discussion, the following quantities are desired in order to comprehensively characterize the samples from the manufacturer:

- 1018MS: $\Delta\phi_{\text{corr}}$, A_{Fe} , A_{H} , and effect of Fe_3C microstructural evolution.
- 304SS: $\Delta\phi_{\text{pass}}$, $\Delta\phi_{\text{breakdown}}$, $\Delta\phi_{\text{pit}}$, and any anomalous polarization behavior.

3 Experimental Procedure

Scan	Soln	Rate	Dir	A_H (V)	A_{Fe} (V)	j_{corr} (A/mm ²)	$\Delta\phi_{\text{corr}}$ (V)
0	H_2SO_4	1 mV/sec	Asc	8.778e-02	8.903e-02	1.784e-06	-4.794e-01
			Des	9.588e-02	8.833e-02	1.888e-06	-4.843e-01
2	H_2SO_4	10 mV/sec	Asc	8.341e-02	8.519e-02	1.663e-06	-4.730e-01
			Des	5.730e-02	8.076e-02	3.096e-06	-4.842e-01
4	HCl	1 mV/sec	Asc	7.706e-02	8.553e-02	1.277e-06	-5.022e-01
			Des	9.978e-02	8.326e-02	1.765e-06	-5.090e-01
6	HCl	10 mV/sec	Asc	7.490e-02	9.225e-02	1.469e-06	-4.806e-01
			Des	1.035e-01	8.415e-02	2.140e-06	-5.097e-01

Scan	Soln	Rate	Dir	j_{corr} (A/mm ²)	$\Delta\phi_{corr}$ (V)	$\sigma^2(j_{corr})$	$\sigma^2(\Delta\phi_{corr})$	n
1	H ₂ SO ₄	1 mV/sec	Asc	1.342e-06	-4.830e-01	6.559e-16	0	338
			Des	1.354e-06	-4.841e-01	3.434e-15	0	421
3	H ₂ SO ₄	10 mV/sec	Asc	2.058e-06	-4.822e-01	2.552e-15	0	342
			Des	1.941e-06	-4.849e-01	1.070e-14	0	444
5	HCl	1 mV/sec	Asc	1.302e-06	-5.032e-01	4.275e-14	0	353
			Des	1.335e-06	-5.085e-01	2.300e-14	0	442
7	HCl	10 mV/sec	Asc	1.265e-06	-4.879e-01	4.494e-15	0	342
			Des	1.297e-06	-4.937e-01	2.720e-14	0	443

Reaction	ϕ_0 (V)	j_0 (A/mm ²)	A (V)	ρ_{lim} ($\Omega\cdot\text{mm}$)
H ⁺ reduction	-3.728e-01	-9.612e-08	-1.138e-01	1.587e+02
Fe oxidation (passivation-limited)	-3.927e-01	7.891e-07	3.505e-03	3.905e+04
Cr ₂ O ₃ barrier breakdown (asc)	9.688e-01	9.902e-07	3.701e-02	1.968e+03
H ₂ O breakdown (asc)	1.596e+00	1.065e-04	2.025e-01	3.230e-312
unknown reduction reaction	1.500e-01	-5.000e-11	-3.289e-02	2.000e+05
Cr ₂ O ₃ solution deposition	1.070e+00	-1.812e+169	-9.784e-06	4.502e+06
Cr ₂ O ₃ barrier breakdown (desc)	9.814e-01	4.565e-07	5.713e-02	1.324e+03
H ₂ O breakdown (desc)	1.599e+00	1.016e-04	1.971e-01	3.765e-06

Reaction	ϕ_{pass} (V)	α_{pass} (V ⁻³)	ρ_{pass} ($\Omega\cdot\text{mm}$)
Fe oxidation (passivation-limited)	-3.530e-01	4.814e+00	6.966e+06
Cr ₂ O ₃ barrier breakdown (asc)	1.300e+00	8.971e-03	5.670e+07
unknown reduction reaction	-3.000e-02	1.000e+01	1.000e+07
Cr ₂ O ₃ barrier breakdown (desc)	1.239e+00	7.470e-03	2.868e+07

Reaction	ϕ_0 (V)	j_0 (A/mm ²)	A (V)	ρ_{lim} ($\Omega\cdot\text{mm}$)
H ⁺ reduction	-3.478e-01	-3.793e-07	-1.145e-01	3.210e+02
Fe oxidation (diffusion-limited)	-4.695e-01	1.498e-08	3.570e-02	2.157e+03
Fe oxidation (passivation-limited)	-4.695e-01	1.498e-08	3.570e-02	2.157e+03
Cl ⁻ ion pitting	3.928e-01	8.802e-05	4.837e-02	9.837e+01

Reaction	ϕ_{pass} (V)	α_{pass} (V ⁻³)	ρ_{pass} ($\Omega\cdot\text{mm}$)
Fe oxidation (passivation-limited)	-1.643e-01	5.187e+03	5.946e+03

Scan	Soln	Rate	Dir	j_{corr} (A/mm ²)	$\Delta\phi_{corr}$ (V)	$\sigma^2(j_{corr})$	$\sigma^2(\Delta\phi_{corr})$	n
1	H ₂ SO ₄	1 mV/sec	Asc	1.342e-06	-4.830e-01	6.559e-16	0	338
			Des	1.354e-06	-4.841e-01	3.434e-15	0	421
3	H ₂ SO ₄	10 mV/sec	Asc	2.058e-06	-4.822e-01	2.552e-15	0	342
			Des	1.941e-06	-4.849e-01	1.070e-14	0	444
5	HCl	1 mV/sec	Asc	1.302e-06	-5.032e-01	4.275e-14	0	353
			Des	1.335e-06	-5.085e-01	2.300e-14	0	442
7	HCl	10 mV/sec	Asc	1.265e-06	-4.879e-01	4.494e-15	0	342
			Des	1.297e-06	-4.937e-01	2.720e-14	0	443

4 Results

5 Discussion

6 Conclusions

7 Acknowledgments

8 Appendix 1: Analysis Code

9 Appendix 2: Surface Microscopy